EUROPEAN LABORATORY FOR PARTICLE PHYSICS

CERN-SL/XX-YYY
Some month, 1999

THE LEP SPECTROMETER PROJECT

The LEP Spectrometer Working Group

C. Bovet[1], W. Coosemans[1], D. Cornuet[1], B. Dehning[1], G. De Rijk[1], G.P. Ferri[1], R. Genand[1], M. Hildreth[1], N. Hilleret[1], W. Kalbreier[1], G. Mugnai[1], Y. Muttoni[1], S. Meyers[1], J. Palacios[2], R. Perret[1], M. Placidi[1], M. Sassowsky[1], E. Torrence[1], R. Valbuena[1], G. Vismara[1], L. Vos[1], J. Wenninger[1], W. Weterings[1], G. Wilkinson[2]

[1]CERN, European Organisation for Particle Physics, CH-1211 Geneva 23, Switzerland
[2]Department of Physics, University of Oxford, Keble Road, Oxford OX1 3RH, UK

Contents

Chapter 1

Overview

The introductory chapter presents the motivation for the LEP Spectrometer Project in the context of the precision electroweak measurents being performed at LEP. The following chapters contain a detailed presentation of the elements of the project: The new dipole (Chapter 3); the spectrometer “arms” (Chapter 4); the necessary instrumentation (Chapter 5); and the Data Acquisition System (Chapter 6). Following this, the results of the 1998 test installation are detailed in Chapter 7. The determination of the integrated bend field of the dipole is presented in Chapter 8. Following this, an outline of the measurement strategy and a summary of the potential systematic errors is given (Chapter 9). The final chapter presents the project schedule and budget.

Chapter 2

Introduction

This section presents an overview of some of the most important electroweak measurements made at LEP, at energies around the Z^0 pole (LEP1) and at higher energies (LEP2). The importance of the beam energy measurement is emphasised, and motivation for a beam energy measurement *at physics energy* at LEP2 is presented. The means for providing such a measurement, the LEP Spectrometer Project, is described.

2.1 Precision Electroweak Physics at LEP

Figure 2.1 shows the physics "landscape" explored by the various phases of the LEP project. LEP1 exploited the peak of the huge Z^0 resonance, resulting in millions of events produced for each of the LEP experiments to study. LEP2 is in the process of exploring an energy regime at more than twice the Z^0 mass, where the pair production of W bosons becomes important. Note that the vertical axis on this figure is on a logarithmic scale; the total rate for e^+e^- annihilation events at LEP2 is roughly a factor of 1000 smaller than at the Z^0 peak.

2.1.1 Specifying the Standard Model

One of the major goals of the LEP physics programme has been to verify (or disprove) the validity of the Standard Model through precision measurements of its fundemental parameters and other physical quantities whose values can be theoretically predicted. In order to do this, a consistent set of definitions must be established in order to relate one measurement to another in the context of electroweak theory. At the simplest level, the three parameters necessary to give the Standard Model predictive power are g (the coupling of the SU(3) Bosons W^1, W^2, W^3 to left-handed fermions), g' (the coupling of the U(1) Boson B to fermions), and $\langle\phi_0\rangle$ (the vacuum expectation value of the Higgs field). There is one caveat, however: since these fundemental constants cannot be calculated from first principles, they must be input from experimental measurements. In addition, these parameters cannot even be measured directly. Instead, combinations of them can be formed which then represent experimetally-measureable quantities. One common choice

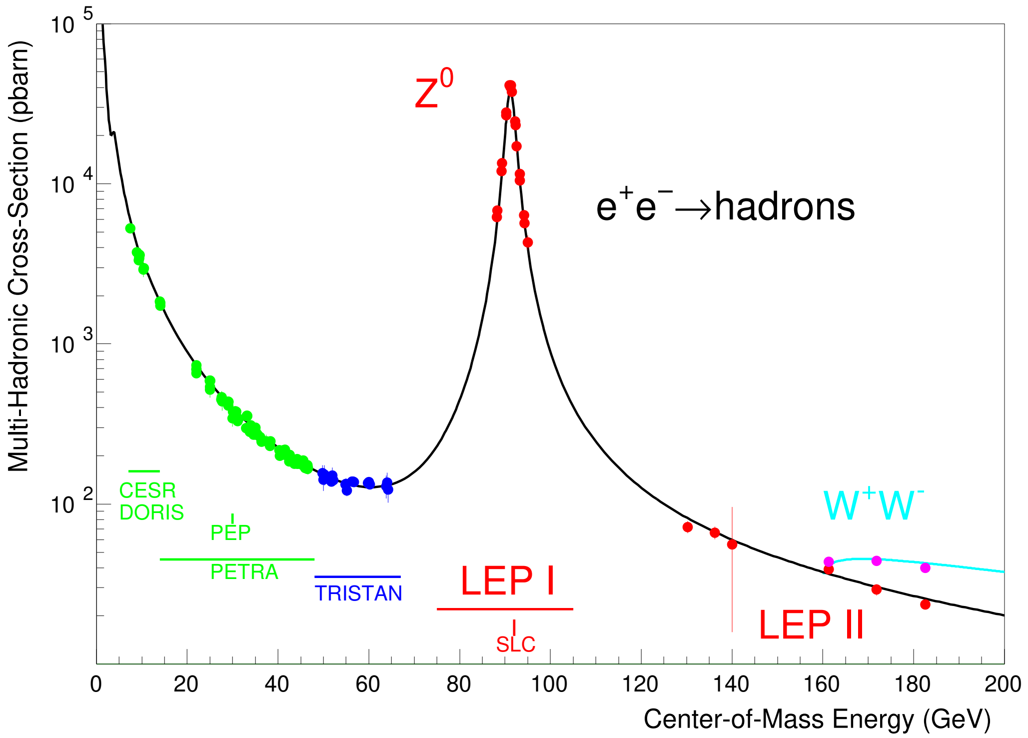

Figure 2.1: The total cross section for hadron production in e^+e^- collisions, showing the prominent features of the energy range covered by LEP. Note the logarithmic scale of the vertical axis.

Quantity			Technique	Precision (PPM)
α	$\equiv$	$\frac{g^2 g'^2}{4\pi\sqrt{g^2+g'^2}}$	$g-2$ of e^- [1]	0.045
G_F	$\equiv$	$\frac{1}{\langle\phi_0\rangle^2\sqrt{8}}$	μ lifetime [2]	17
M_Z	$\equiv$	$\frac{1}{\sqrt{2}}\langle\phi_0\rangle\sqrt{g^2+g'^2}$	Z^0 lineshape [3]	22

Table 2.1: Three experimentally measured constants which can be used to specify the numerical predictions of the Standard Model. Their relationship to fundemental electroweak parameters and the relative precision with which they are known are also given.

of three measurements used to specify the theory is $\alpha_{EM}(M_Z^2)$, G_F, and M_Z. There relationship to the three fundemental electroweak parameters, the means by which they are measured, and the relative precision with which the are known are given in Table 2.1.

Once these input parameters are measured with sufficienct precision, their values can be used to predict other combinations of the fundemental constants. For example,

$$M_W = \frac{1}{2} g \langle \phi_0 \rangle$$

and

$$\sin^2 \theta_W = \frac{g^2}{g^2 + g'^2}$$

2.1.2 Testing the Standard Model

It should be noted that the relationship between the measured quantities and the fundemental parameters shown here is strictly valid only to lowest order in the theory. Beyond this, higher-order corrections introduce a dependence of the parameters on the top and Higgs masses, and, potentially, the masses of yet-undiscovered particles. If the input parameters are sufficiently precise, the effects of the radiative corrections themselves can be studied. This formed the thrust of the LEP1 programme, where M_Z was measured with a relative precision of 3×10^{-5}. This enabled the use of other measurements, like that of $\sin^2 \theta_W$, to correctly predict the value of the top quark mass m_t based solely on the effects of radiative corrections.

At LEP2, another precision test of the Standard Model is within reach. As shown above, the value of the W boson mass (M_W) is also predicted within the Standard Model. A measurement of M_W not only serves as an additional verifcation of the underlying theory, but, since the top quark mass is now known, it also provides information on the Higgs sector. This is shown in Figure 2.2, where the Standard Model predictions for the W and top quark masses are compared with the direct measurements from LEP and the Tevatron. Because of the radiative corrections, both M_W and m_t are related to the Higgs mass; the predictions of this interrelationship for various Higgs masses is also shown.

When the value of the top quark mass is taken into account, the precision of the prediction for the W mass based on low-energy data is approximately 33 MeV. Thus, the goal of the LEP2 programme is to produce a measurement of M_W with an experimental error of this size or smaller in order for a comparison with the electroweak theory to be meaningful.

2.2 Measurements of M_W at LEP

At LEP2, two techniques are available for measuring the W mass. The first, a measurement of the W-production cross section very close to the kinematic threshold for W-pair production, was exploited in 1996 to provide the first M_W measurement from LEP[4]. The second method, based on a reconstruction of the W mass from the kinematic properties of the events, is the only applicable technique far above the W production threshold[5], since at these higher energies the production cross section is insensitive to the precise value of the W mass. Figure 2.3 shows the measurements of the W-pair production cross section as a function of energy from the LEP experiments. Figure 2.4 shows an example of the mass peaks obtained from the direct reconstruction method.

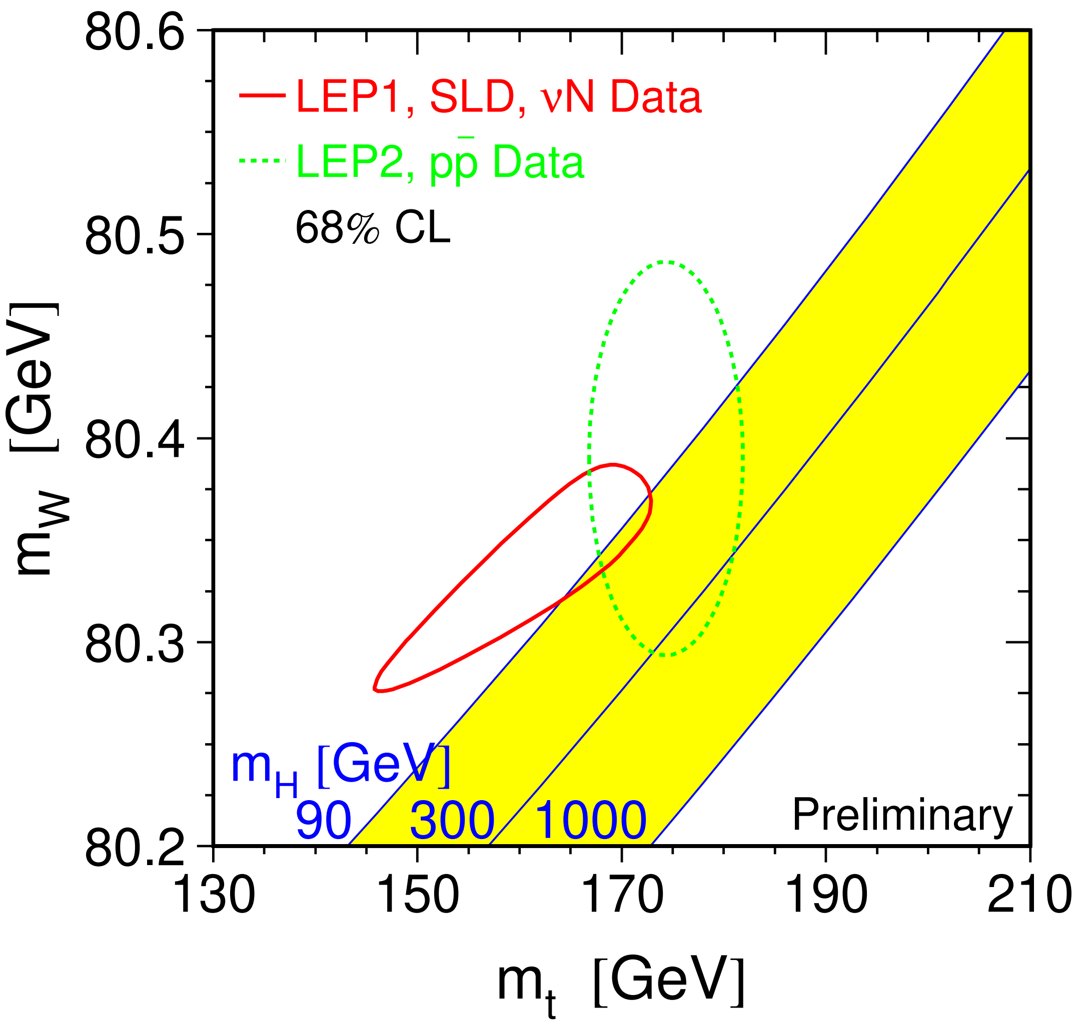

Figure 2.2: A comparison of the predicted and measured values of the W boson and top quark masses. The predicted values are derived from low energy measurements, including data from the Z pole, neutrino scattering, and atomic parity-violation experiments[3].

2.2.1 Errors on the M_W Measurement

For the canonical integrated luminosity of 500 pb^{-1} per experiment, the statistical error on M_W should reach 25 to 30 MeV. Thus, in order for the total experimental error to reach the target of approximately 35 MeV, the experimental systematic errors need to be controlled at or below the 10-15 MeV level.

A potentially large source of systematic error is that due to the uncertainty on the LEP beam energy. In either technique for measuring the the W mass, the beam energy is used to set the absolute scale of the measurement. The W mass error, δM_W, is essentially

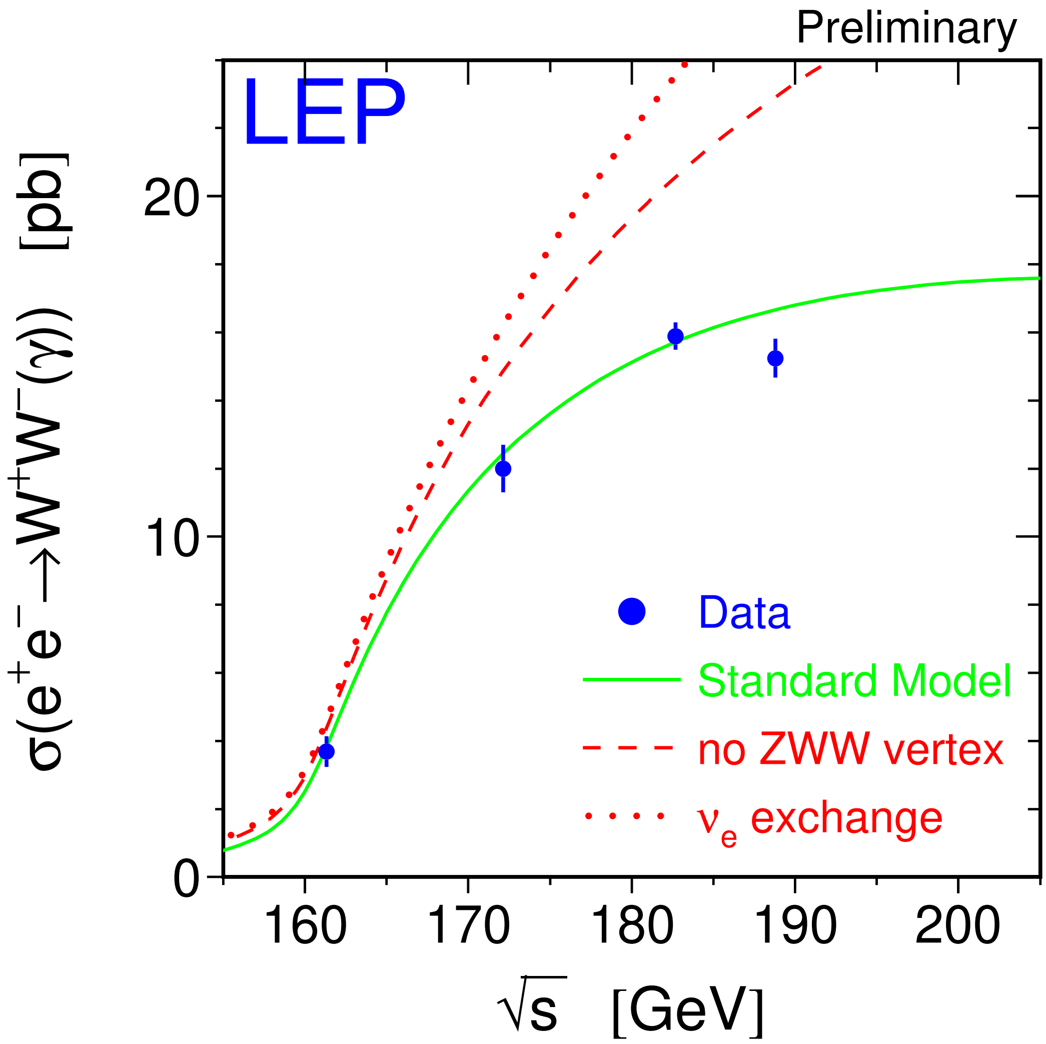

Figure 2.3: The measured values of the W-pair production cross section as a function of centre-of-mass energy. The points show the combined measurements of the four LEP experiments; the curves show the standard electroweak theory and some representative models which lack crucial elements of the Standard Model.

linearly proportional to the beam energy error δE_{beam}:

$$\frac{\delta M_W}{M_W} \approx \frac{\delta E_{beam}}{E_{beam}}.$$

The current technique for determining the beam energy and the prospects for achieving the required level of uncertainty are described in the next section.

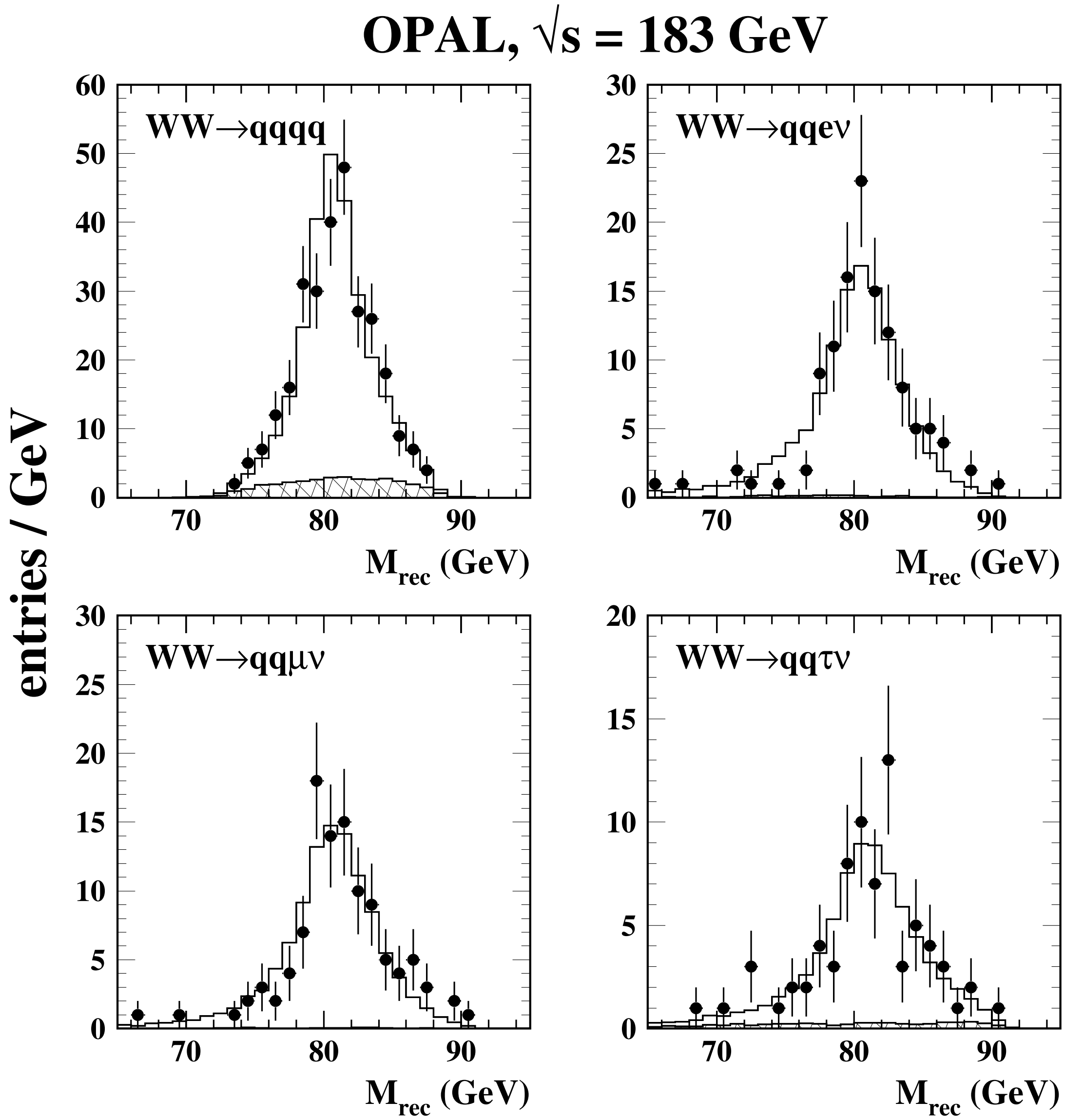

Figure 2.4: The reconstructed mass distributions for data taken at 183 GeV by the OPAL experiment[6]; the peaks at M_W can clearly be seen. Separate plots are shown for the different final states in W decays: a) $WW \to qqqq$ events; b) $WW \to qqe\nu$; c) $WW \to qq\mu\nu$; and d) $WW \to qq\tau\nu$ events. The hashed region on each plot is the calculated background.

2.3 The LEP2 Beam Energy Measurement

The LEP2 beam energy measurement is described in great detail in [7] and is summarised here. As at LEP1[8], the determination of the total bend field provided by the magnetic elements of LEP is the primary part of the measurement. The technique of resonant depolarisation[9], however, cannot be used at physics energies because of depolarising

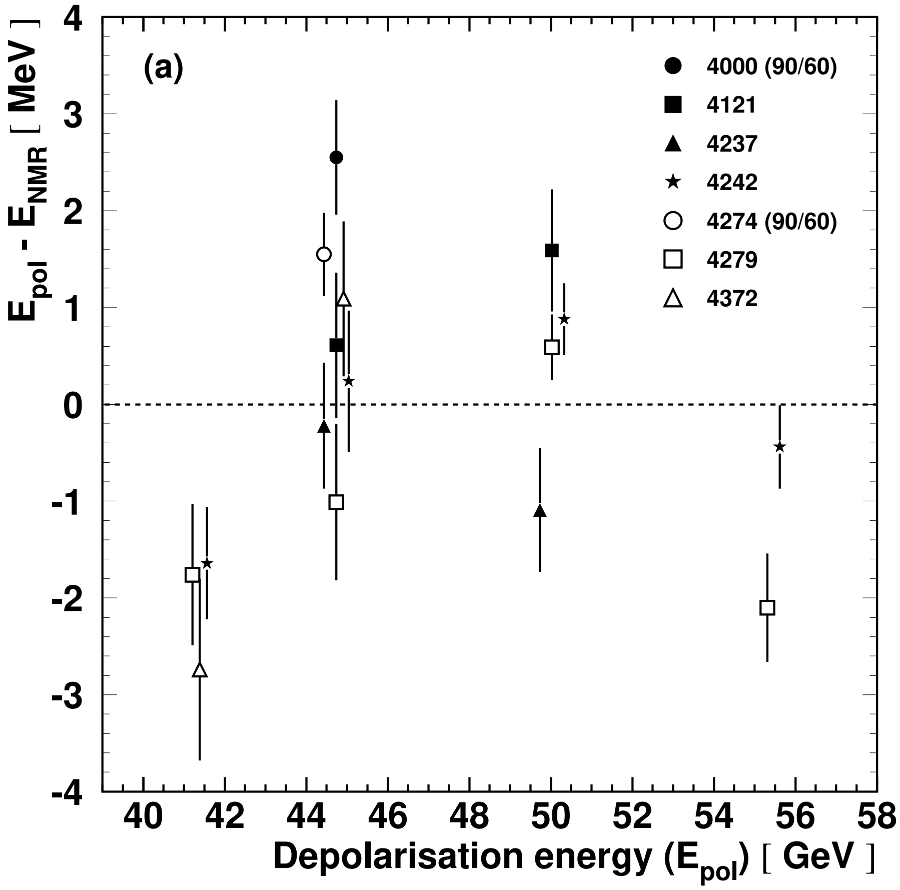

Figure 2.5: Residuals of the fit comparing resonant depolarisation energies to the energies predicted by the NMRs for a simultaneous fit to all 1997 fills with polarisation measurements. For clarity, the points for different fills have been plotted at slightly displaced depolarisation energies.

effects that increase strongly with beam energy. Instead, resonant depolarisation measurements made at lower energies (up to 55 GeV for 1997) are used to calibrate alternate measures of the total bend field, namely 16 NMR probes installed in the LEP dipoles. The relationship between the bend field measured by the NMRs and the true beam energy is assumed to be linear (as is measured over the limited range of energy that they can be compared, see Figure 2.5), and the bend field measured in physics conditions is used to determine the beam energy. The assumption that the relationship between the true beam energy and the measured bend field remains linear at energies above where they can be compared is crucial to the analysis.

As at LEP1, other corrections need to be applied to the purely dipole contribution to the total integrated bend field in order to obtain the true beam energies at each LEP interaction point. Some of them, such as the correction due to the earth tides, can be large, of order 40 MeV. Of particular relevance to our discussion here is the correction due to the energy variation around the LEP ring caused by energy loss to synchrotron radiation, and the corresponding energy gain from the RF acceleration system. Overall shifts of the centre-of-mass energies at the interaction points tend to be small, of order 20 MeV or so, but the beams can deviate by more than 400 MeV from their average energy while traversing each LEP arc. This will be important when extrapolating the energy of a single beam to a particular point along the LEP ring.

2.3.1 Systematic Errors on the Beam Energy Measurement

Table 2.2 shows the current evaluation of the systematic errors on the beam energy at LEP2, as determined in the method described above[7].

Source	Error [MeV]
Extrapolation from NMR–polarisation:	
NMR rms/$\sqrt{N}$ at physics energy	10
Different E_{pol} fills	5
Flux-loop test of extrapolation:	
NMR flux-loop difference at physics energy	20
Field not measured by flux loop	5
Polarisation systematic	1
e^+e^- energy difference	2
Optics difference	4
Corrector effects	3
Tide	1
Initial dipole energy	2
Dipole rise modelling	1
IP specific corrections ($\delta E_{\mathrm{CM}}/2$):	
RF model	4
Dispersion	2
Total	25

Table 2.2: Summary of contributions to the 1997 beam energy uncertainty.

As can be seen from the table, the dominant systematic error arises from the one cross-check of the linear extrapolation assumption that is currently available, namely, a comparison between the field measured locally by the NMR probes and that measured by the flux loop. To make this comparison, the extrapolation procedure is repeated, using the flux loop, which measures 96.5% of the total dipole bend field of LEP, as the

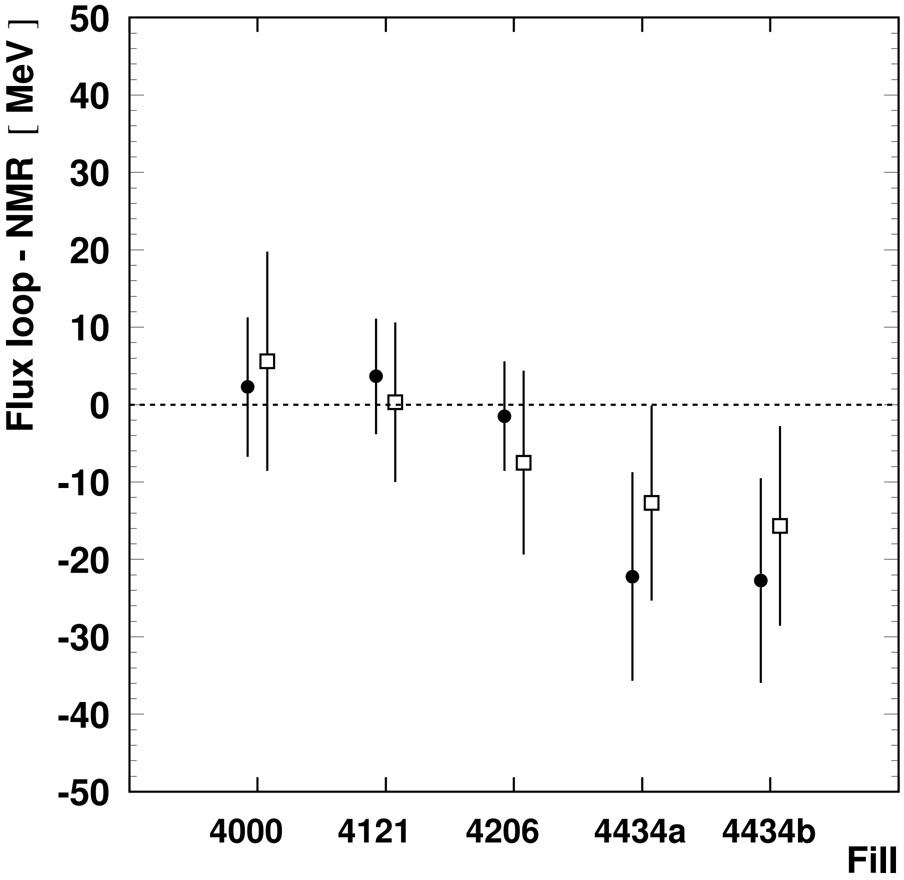

Figure 2.6: The difference (scaled by 92.9 MeV/Gauss) between the magnetic field measured by the flux loop and predicted by the NMR probes at physics energy (91.5 GeV) for each flux-loop measurement in 1997. The solid points are for all working probes for each fill, while the empty points are for the common set of probes working for all fills.

"true" beam energy against which the NMRs are calibrated. The calibration is performed over the same energy range (beam energies less than 55 GeV) as for the method using resonant depolarisation. Since both devices can measure the magnetic field over the full range of LEP energies, however, a comparison of the field measured by the flux loop and that predicted using the NMR calibration determined at lower energies yields an estimate of the "bias" of the extrapolation method. For the 1997 analysis, this bias varied by approximately 20 MeV throughout the year, as shown in Figure 2.6. Since the source of the time-dependence of this variation is not understood, the entire variation was taken as the error. The overall error of 25 MeV is substantially larger than the target of 10-15 MeV. In addition, the as-yet-unpublished data from the 1998 running show a similar variation[10]; unless the understanding of the accuracy of the flux loop measurement and its potential errors improves dramatically in the near future, there is little hope to reduce the error from the extrapolation method to the desired level.

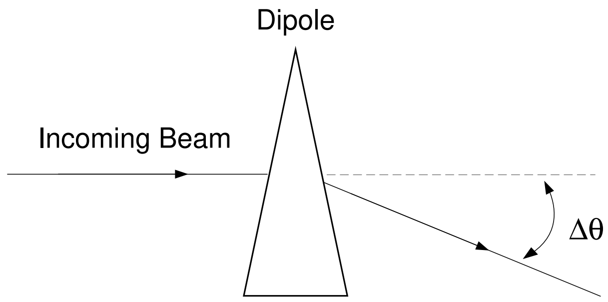

Figure 2.7: The spectrometer principle.

2.4 The LEP Spectrometer Project

The considerations of the following section concerning the apparent irreducibility of the extrapolation error, plus the concern that both the actual measurement and the only cross check rely on imperfect estimates of the total bend field of LEP led us to propose in the Fall of 1997 the LEP Spectrometer Project. This simple device will allow an actual *measurement* of the beam energy at physics settings and thus will sidestep completely any problems in estimating the total bend field, etc.

2.4.1 The Concept

The simplest means of measuring the energy of a particle beam is to bend it with a known magnetic field, and measure the bend angle, as shown schematically in Figure 2.7.

For a simple spectrometer, the beam energy is given in terms of the integral bend field of the bend magnet ($\oint B \cdot d\ell$) and the measured bend angle ($\Delta\theta$) by

$$\Delta\theta \propto ???\frac{\oint B \cdot d\ell}{E_{beam}}$$

Due to the limited space available in LEP, the "classic" spectrometer, in which the magnetic field of the spectrometer magnet does not change, is impossible. Instead, a slightly different design has evolved, where the spectrometer magnet provides part of the bend field of LEP and hence ramps with the rest of the dipoles as the energy of the machine is increased. This implies that the bend angle $\Delta\theta$ is *fixed.* In order to allow for continuous measurement in the high-radiation environment of LEP2, beam positions monitors (BPMs) are used to measure the incoming and outgoing trajectory of the beams, so that the overall layout of the spectrometer appears like that shown in Figure 2.8.

2.4.2 Tolerances/Requirements

The design goal of the Spectrometer Project is to provide an energy measurement with a relative precision of 10^{-4}, or 10 MeV beam energy error at 100 GeV. Once the geometry

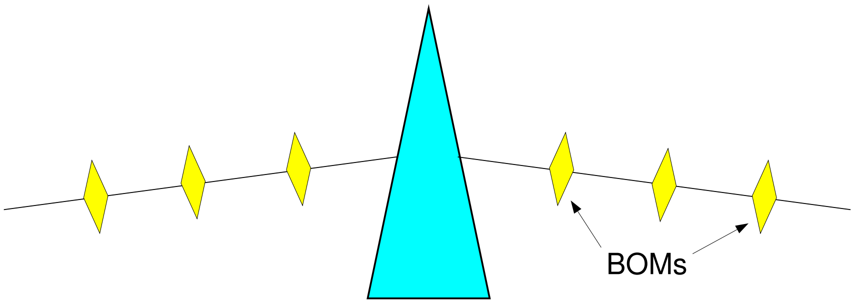

Figure 2.8: The layout of the LEP spectrometer, showing a single dipole magnet surrounded by BPMs.

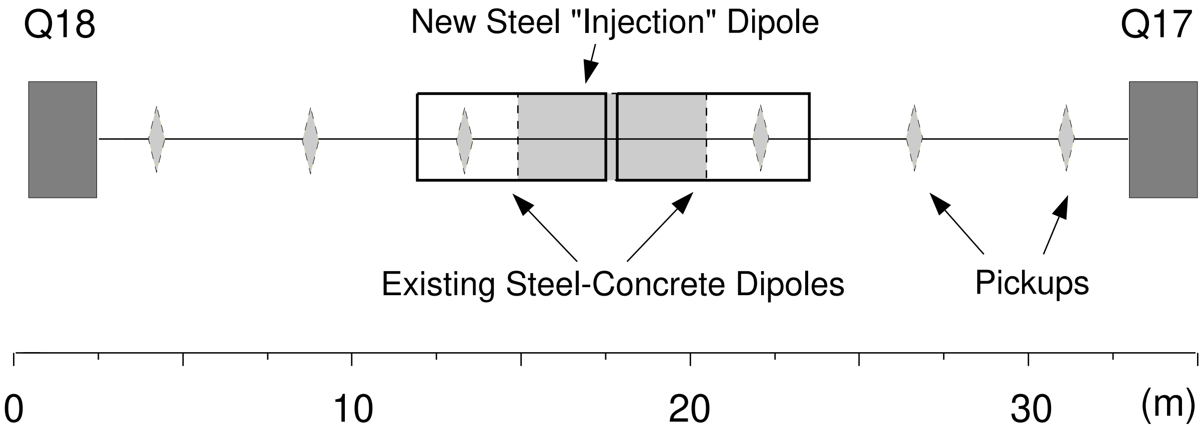

Figure 2.9: A schematic of the LEP spectrometer layout in its location in the LEP tunnel. The quadrupoles in the dispersion suppression section and the existing concrete dipoles are shown. In dotted lines, the approximate locations of the new dipole magnet and the BPMS are also shown.

of the layout is fixed, this precision determines the relevant tolerances on stability and resolution in a straightforward manner.

There exist 16 places in the LEP lattice where a bend magnet is surrounded by sufficient drift space for a spectrometer installation. In the dispersion suppression sections surrounding each interaction point, between Q17 and Q18, two standard concrete-iron dipoles provide a bend of 3.8 mrad and are surrounded by approximately 8 meters of drift space, as shown in Figure 2.9. The spectrometer installation will replace these dipoles with a single, double-strength dipole whose field has been precisely mapped at different energies, and the necessary BPMs will be installed on either side.

Given this layout geometry, then, the necessary resolution on the horizontal position measurement for the BPMs can readily be calculated. The relative precision of the angle measurment for two spectrometer "arms" of three BPMs each is shown in Figure 2.10 as a function of the arm length and the single BPM resolution. It can easily be seen that an

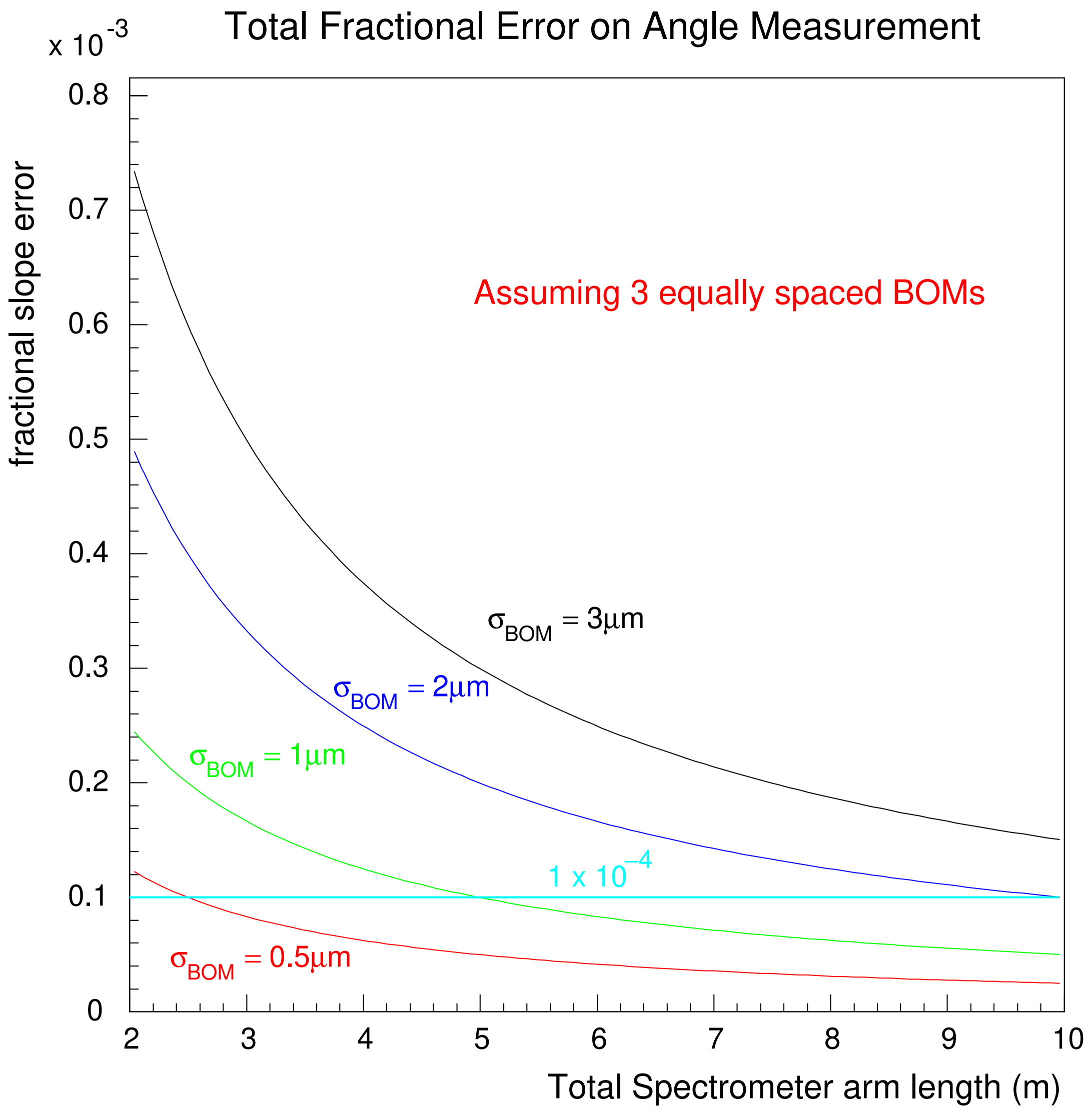

Figure 2.10: A schematic of the LEP spectrometer layout in its location in the LEP tunnel. The quadrupoles in the dispersion suppression section and the existing concrete dipoles are shown. In dotted lines, the approximate locations of the new dipole magnet and the BPMS are also shown.

angle measurement of better than 10^{-4} requires a single BPM resolution of order 1 micron and an arm length of at least 5 meters or so. Since the *total* measurement error should be 10^{-4}, an error of $5-7\times10^{-5}$ is allowable for the uncertainty on the BPM measurement, which is compatible with 1 micron resolution and a 6 to 7 meter arm length.

The next two sections present an overview of how the necessary precision on the magnetic field map and the BPM resolution will be achieved. Detailed consideration of these points will be presented in the following chapters.

2.4.3 Measurement of the Magnet Field Integral

In order to achieve the desired precision on the energy measurement, the relative change in the dipole field integral must be known to better than 10^{-4}[1]. For reasons given in Chapter 3, it was decided that only a steel dipole would be sufficiently stable to meet this requirements. The field map itself was carried out with a precision mapping bench in the ISR tunnel. The mapping setup and procedure is described in detail in Chapter 8. Maps of the magnetic field were made using a moveable carbon-fibre arm equipped with an NMR probe and two Hall probes. The Hall probes were used primarily to measure the end fields, since NMR probes cannot be used in regions with high field gradients. Position resolution of Z microns per measurement was achieved using a special encoded ruler with optical readout. The temperature coefficient of the magnetic field at different excitations was determined by mapping the field at different magnet core temperatures. The coefficient itself is XXXX at a current equivalent to 41 GeV beam energy, and changes to YYYY at 100 GeV. In order to mitigate field changes from temperature effects, a special cooling circuit for the dipole coils and the section of beampipe inside the magnet has been desiged (see Section 3.3). This should control fluctuations of the magnet core temperature to $\pm 1^\circ$ C, resulting in small (but measured) corrections to the field integral. The estimated total error on the ratio of the field integrals between 44 and 100 GeV is BBBBB. A detailed error summary is given in Section 8.3.

2.4.4 The BPM Position Measurement

The requirement of a $5-7\times10^{-5}$ measurement of the bend angle translates into a necessary resolution of approximately 1 micron per BPM measurement. This is the *total* resolution on the position measurement, including mechanical stability, electronic drift, and the intrinsic resolution of the orbit measurement itself. In order to meet these requirements, several components are needed:

- BPM electronics with stable resolution on horizontal beam position of $< 1\ \mu$m
- a special beam pipe with flexible bellows for vibration isolation and collimators to protect the BPMs from synchrotron radiation
- a mounting for BPM/beampipe assembly that is stable to much better than a micron
- a special cooling circuit to maintain a constant BPM temperature to $\sim 0.2^\circ$ C
- Position verification with sub-micron resolution to monitor any relative motion between the BPMs

[1] Only the *relative* change in field integral is needed because the BPMs do not provide an absolute position measurement. The Spectrometer energy scale must be calibrated against the energy from a resonant depolarisation measurement at lower energy. In actuality then, the Spectrometer provides an energy measurement *relative* to that given at a lower energy.

In addition to these requirements, the entire system must be stable for the time required to make the actual measurement, which will be at least two hours.

For the BPM electronics, a design of the BERGOZ company has been chosen. This is a modified version of BPM electronics which have achieved stable, sub-micron resolution is synchrotron light sources[11]. As is discussed in Chapter 7, a preliminary version of the Spectrometer BPM electronics achieved a single-BPM resolution of 0.7 microns in the test installation, albeit in a non-optimal operating mode. The mechanical design for the beam pipe, collimators, bellows, and their accompanying supports and cooling system performed well in the test installation, and are described in detail in Chapter 4. A stretched carbon-fibre position monitor system was chosen to measure any change in position between the BPM stations, both along each Spectrometer arm and between each of the arms (see Chapter 5). It achieved a resolution of some 200 nanometers, but suffered from large systematic effects induced by the synchrotron radiation from the LEP beams. Its performance and these other effects are also discussed in Chapter 7.

Chapter 3

The MBI Dipole

Three considerations led to the decision to replace the concrete-steel dipoles with a new steel dipole. First, the stability of the concrete-steel dipoles, both in terms of the temperature dependence of their magnetic fields and their "ageing" characteristics, is not sufficient to obtain the needed precision. The steel magnets of the type found in the injection regions of LEP have shown better field stability, better temperature behaviour, and should not age. Second, using these dipoles would require mapping both of them, which is impractical given the time constraints of the project. Third, once it was clear that a steel dipole would be needed, it was determined that purchasing a new magnet was less expensive than exchanging the two steel-concrete dipoles for an existing steel dipole in the LEP injection region. This also allowed the correction of a flaw in the pole-tip shape of the original injection dipole design (see Section 3.2).

This chapter presents a description of the mechanical design of the MBI dipole assembly, including its support girder and cooling circuit.

3.1 Mechanical Design

3.1.1 The MBI Magnet

3.1.2 The MBI Support Girder

3.2 Magnetic Design

3.3 Magnet Cooling

Chapter 4

The Mechanical Design

As was discussed in the Introduction, the mechanical stability of the BPM support is of paramount importance in maintaining the required resolution of the position measurement. In addition, the BPMs must be shielded from synchrotron radiation to eliminate both the additional heat load and potential electronic effects from photons hitting inside the BPMs themselves. This chapter concentrates on a description of the BPM stations, including their supports, shielding, and cooling. At the end of the chapter, the modifications to the LEP vacuum system necessary for the Spectrometer installation are described, and an overview of the entire Spectrometer layout is given.

4.1 The BPM/Absorber Assembly

The installation of BPMs in the Spectrometer occurs in six identical BPM "stations" consisting of a single pickup surrounded by two protective copper collimators known as "absorbers." The following sections present the mechanical design of the BPM station in detail, including the motivation for particular choices of mechanical structure and materials.

4.1.1 BPM Hardware

The BPM measurements are made using a standard LEP "dipole" BPM block, fabricated from aluminum. These pickup blocks are oval in cross section; the major axis of the oval is 125? mm, the minor axis 90? mm. The four buttons which sense the induced voltage left by the passing beams lie on the diagonals, as seen in Figure 4.1. The aluminum blocks were chosen over the round, stainless-steel "quadrupole" blocks because, even though the thermal expansion coefficient of aluminum is nearly twice as large, the thermal conductivity of aluminum is better than that of stainless steel. The blocks themselves are individually cooled to take advantage of this; the additional cooling tubes, routed through a copper block for better contact, can be seen in Figure 4.1. Additional holes have been drilled in the blocks for mounting them on a more stable support and for supporting the sensors for the stretched-wire system.

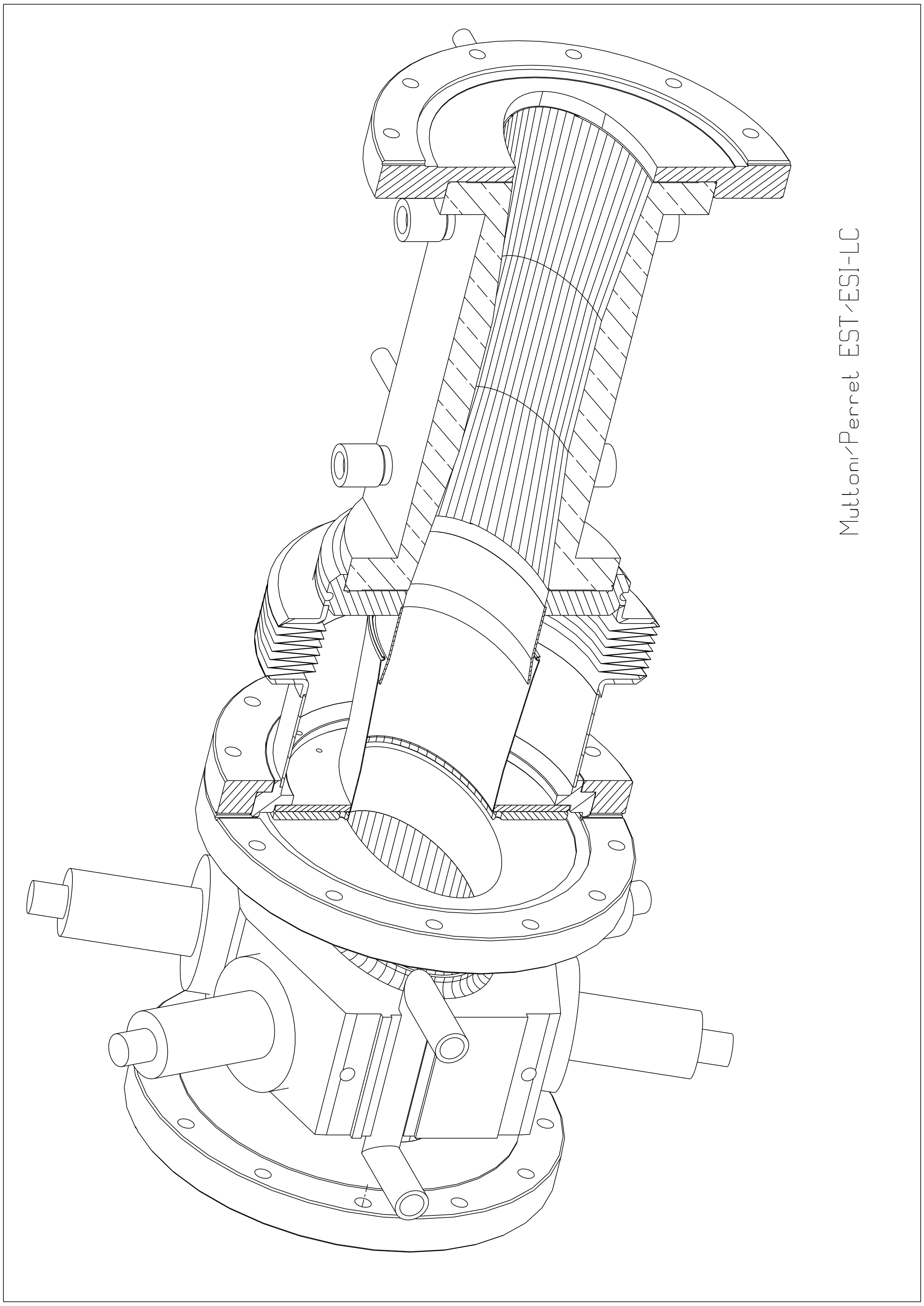

Figure 4.1: A drawing of the cross-section of a standard oval "dipole" BPM block. The four button pickups are labelled "A", "B", "C", and "D". Of particular note is the addition of a copper block containing a cooling channel so as to better regulate the temperature of each BPM.

4.1.2 The Absorbers

In the LEP arcs, the energy deposited by synchtrotron radiation can reach nearly 1 kW/meter, as shown in Figure **??**. If this energy were to impinge on the aluminum BPM block, any hope of mechanical stability would be lost; the BPM block would undergo many microns of motion from thermal expansion and contraction. In addition, there is the worry that photo-electrons generated by the synctrotron light hitting the pickup buttons could render the pickup useless. Originally, it was hoped that there were enough spare moveable collimators available that could be used to protect the BPMs. When this turned out not to be the case, individual, copper "absorbers" were suggested, to be installed on either side of each pickup. The absorbers are tapered to reduce HOM effects, and elliptical in cross section to match the pickup blocks. The BPM/Absorber assembly can be seen in Figure 4.2. Note the flexible bellows which has been welded between the pickup and the absorber. This has been added to further decouple any motion of the absorbers as they are subject to large thermal fluctuations.

These fixed copper collimators absorb more than 99% of the synchrotron light that would have struck the BPMs. Thermal studies of the absorber structure, assuming an energy depostition of 2 Watts/mm^3 in the horizontal, primary synchrotron fan and 1 Watt/mm^3 (????) everywhere else showed that the temperature rise of the absorber could be controlled using the standard LEP cooling water circuit, and this was tested during the 1998 running. Examples of their temperature excursions are shown in Section 4.1.4.

4.1.3 A BPM Station

Figure 4.3 shows the BPM/Absorber assembly as it is installed in LEP. Each BPM station sits on its own Jurassic limestone block, which is grouted to the tunnel floor. The BPM block and the two absorbers are mounted independently, so that the only mechanical coupling between the pickups and the aborber blocks is through the flexible bellows or the limestone block.

The BPM mounting assembly is shown in Figure **??**. Effectively, each pickup is "sandwiched" between parallel stainless steel??? plates, which are then fixed to a flat base. Three screws control the vertical and tilt adjustments; a fourth screw affixed to another plate serves to "block" the position adjustments by holding the assembly fixed.

4.1.4 The BPM Cooling System

Given the thermal expansion coefficient of the BPM blocks ($\Delta L/L \approx 2.5 \times 10^{-5}/°C$), it is clear that the standard LEP cooling water circuit is inadequate to maintain the desired temperature stability, since its temperature changes by many degrees during a LEP fill. In addition, since the BPMs themselves do not represent a large thermal load, it is relatively straightforward to purchase a standalone cooling system to regulate their temperature. To further isolate the BPMs from the surrounding environment, a box of insulating material is placed over each BPM station.

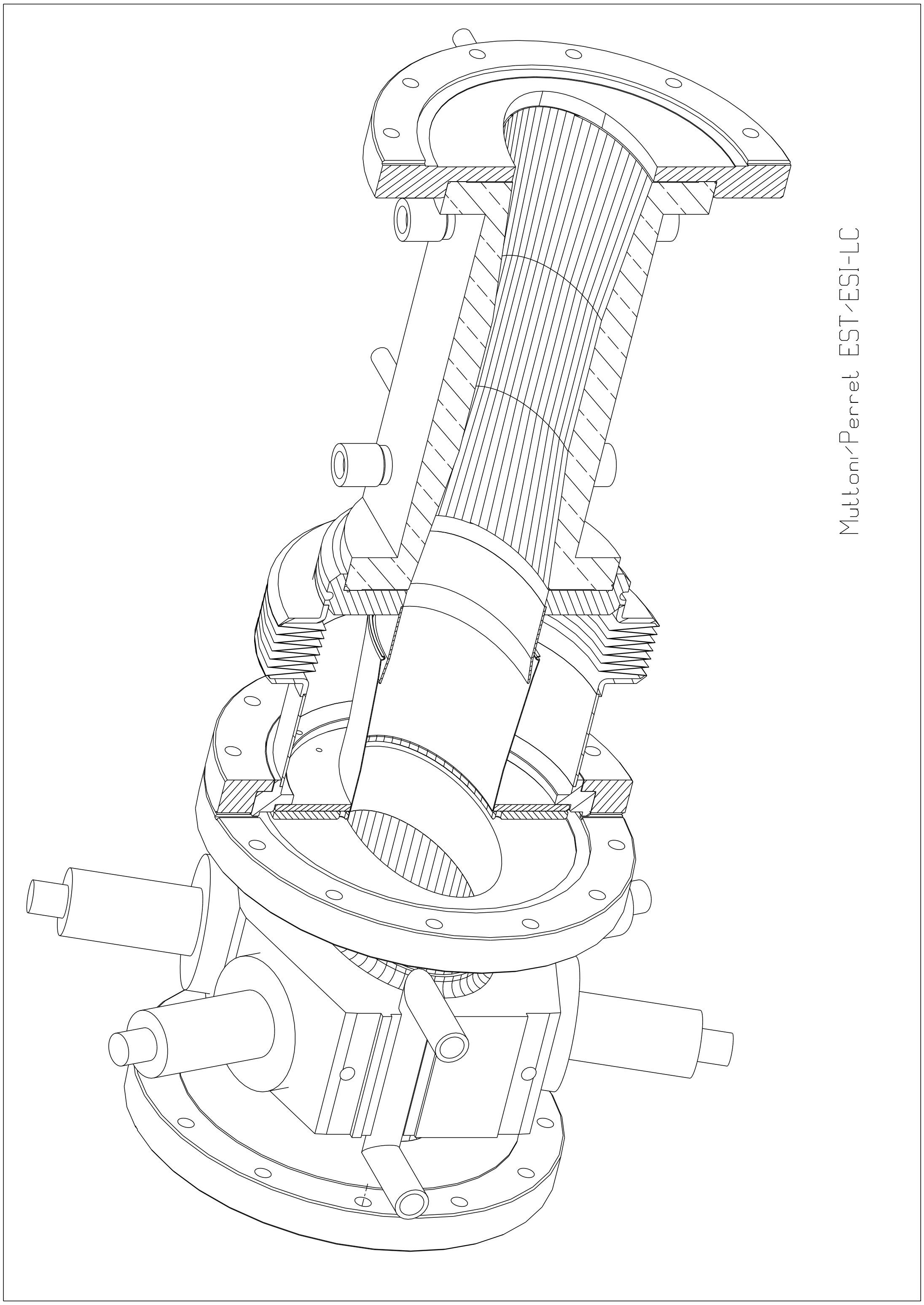

Figure 4.2: A drawing of the pickup/absorber assembly, showing a cross-section of the absorber, where the tapered structure can clearly be seen.

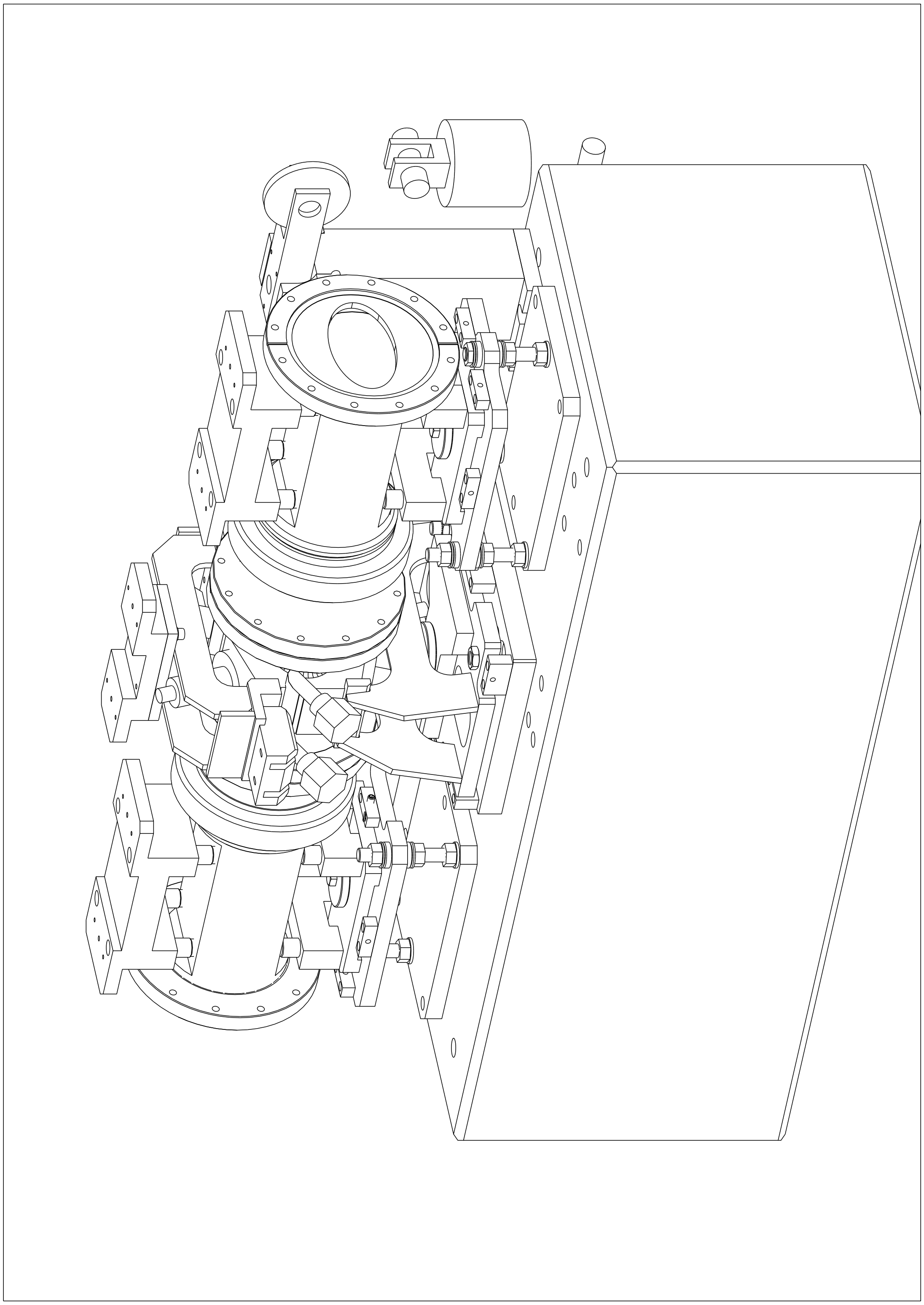

Figure 4.3: A drawing of a single BPM station, showing the BPM block itself, the surrounding bellows and absorber assemblies atop the limestone block.

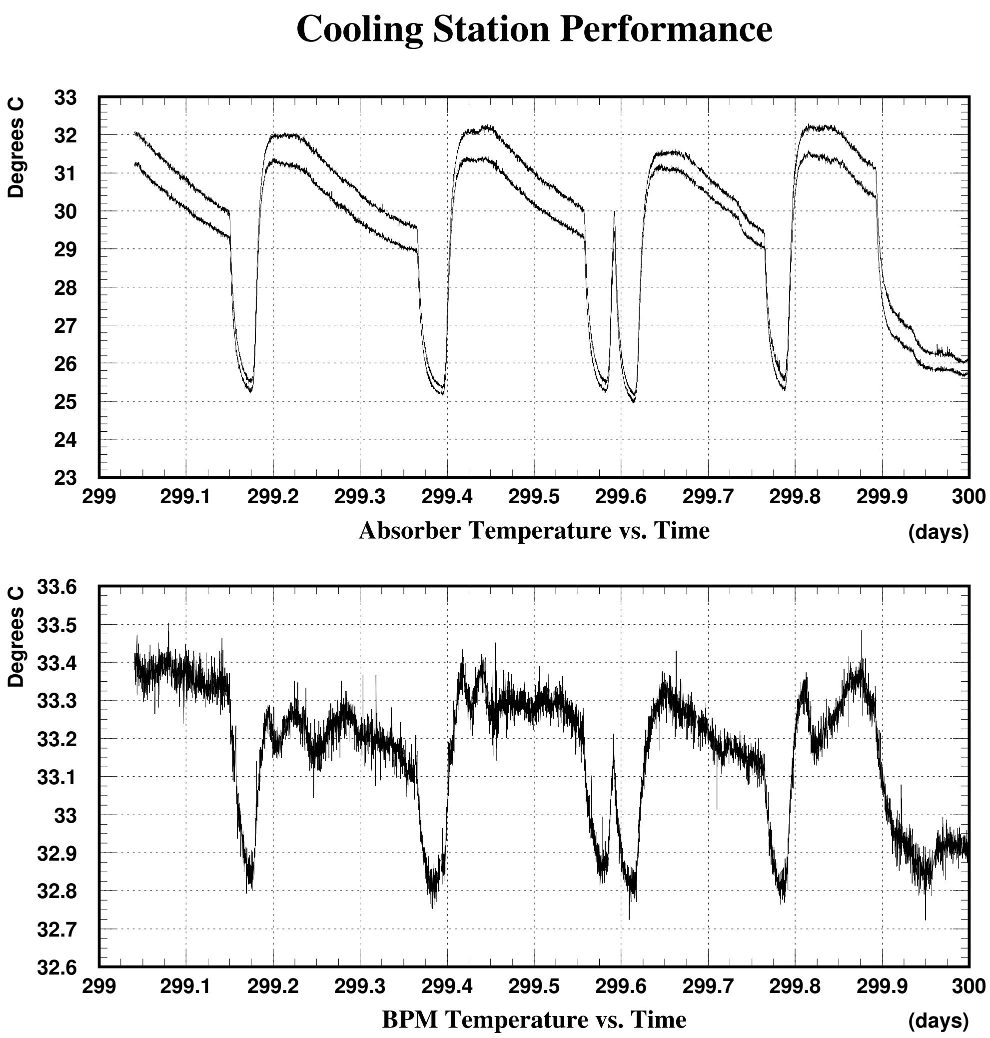

Figure 4.4: A time history of the temperatures measured on the copper absorbers (upper plot) to the left and right of the middle BPM in the test installation, and the temperature measured on the BPM block itself (lower plot). Note that the vertical scale is a factor of ten smaller on the lower plot, clearly showing the effectiveness of the temperature regulation provided by the cooling station.

The layout of the BPM cooling circuit is shown in Figure **??**. Figure 4.4 shows the performance of the system during physics running in 1998. The lower plot shows the temperature measured on the copper absorbers on one of the pickup stations. The upper plot shows the temperatures measured simultaneously on the BPM block. The excellent temperature stability of the pickups in the high intensity synchrotron radiation environment can clearly be seen.

4.2 The Vacuum System

Some modifications to the vacuum system were necessary for the Spectrometer installation. In particular, customised versions of the standard LEP "dipole" chamber with connection flanges removed from the horizontal plane were needed in order that the stretched-wire system did not encounter any mechanical interference. In addition, as many magnetic or magnetisable elements as possible were removed from the vacuum chamber construction. The insertion of the BPM stations represents a loss of approximately 9 meters of getter pump where the Spectrometer is installed. This is not expected, however, to pose any problem in maintaining the vacuum quality in this region of LEP.

4.3 The Spectrometer Layout

Figure **??** shows the actual layout for the Spectrometer installation in half-cell 332, left of IP3. Out of the sixteen possible locations, this one was chosen because it avoided the effects of the LHC construction, it is close to an alcove where cables can be run, and there is little other beam instrumentation nearby. As can be seen from the figure, each spectrometer arm has a length of approximately 7 meters.

Chapter 5

Instrumentation

This chapter presents a description of the extensive instrumentation installed in the Spectrometer, both to make the actual energy measurement and to monitor as many environmental variables as possible, as this is the only way the systematic errors can be controlled.

5.1 The BPM Electronics

5.2 The Stretched Wire System

In order to monitor any relative change in the physical positions of the BPMs, some sort of reference is needed, whether it be mechanical or optical. The resolution of the reference system must be substantially better than 1 micron so as to not add too much additional position error to the BPM measurement. Extensive experience gained at the CLIC Test Facility with stretched wire systems[?] and the difficulties and expense of setting up a stable optical system over the 30 meter length covered by the Spectrometer led to the choice of a stretched wire system to provide the necessary reference for the Spectrometer. The entire system has been purchased from FOGALE.

The stretched wire itself is a kapton-coated carbon fibre filament with a huge tensile strength, but a mass per unit length of only 300 grams/kilometer. Wires pass through one passive capacitive sensor on each side of each BPM, as shown in Figure **??**. The sensor heads chosen for this project provide both the horizontal and vertical positions of the wire; a sensor head is shown in Figure **??**. Pre-amp electronics are located within several meters of the sensor heads themselves. The amplified voltages are also measured by a Keithley XXXXX Digital Voltmeter. Typically, a one mV variation corresponds to 1 micron of relative motion between the sensor and the wire.

The geometry of the reference wires was chosen to provide the maximum information on any deformation of each pickup block due to thermal expansion, while maintaining the needed "straight line" reference between the two arms of the spectrometer. With this configuration, any net rotation of one arm with respect to the other around the center of the magnetic bend can be measured.

Each of the three wires includes a "reference" sensor at each end to compensate for any motion of the wire supports. In this way, any differential motion between the reference sensors and those on the pickup blocks can directly be attributed to motion of the pickups. The reference sensors themselves are mounted on stands with an extremely small thermal expansion coefficient, made from carbon fibre, in order to provide as immoveable a reference as possible. Figure **??** shows a reference sensor next to the pulley-counterweight mechanism used to maintain constant tension on the carbon fibre wire.

The resolution of the wire system, as measured during stable conditions during the 1998 running, is excellent, of order 200 nm or so. Unfortunately, the sensor heads appeared to be susceptible to the harsh synchrotron radiation in LEP, and large non-physical variations in the wire positions were seen as the beams were ramped to high energy or when the beams were dumped. The performance and these problems are discussed in more detail in Chapter 7.

5.3 Temperature Measurements

One of the most difficult aspects of the Spectrometer project is maintaining mechanical stability in the face of the large temperature changes that occur when LEP is ramped to high energy. Hence, the monitoring of the temperature of each critical component is crucial to the success of the project. To this end, approximately 60 PT100 (cite?) temperature probes have been installed in and around the Spectrometer. These include one probe on each wire sensor, one on each side of each BPM, approximately 20 on various positions on the MBI dipole, and a number measuring the ambient temperatures as well as those of the electronics. A complete list is given in Table **??**. The excellent resolution of the Kiethley DVMs far outpaces what is needed for temperature monitoring, but it was simplest to merely add the temperature probes to the system used for the BPMs and the wire system.

5.4 Other Instrumentation

Flux Gate... ?

Chapter 6

The Data Acquisition System

6.1 The “Belowline” System

Kiethley’s, OS9...

6.2 The “Online” System

HP-UX, data pool...

6.3 Databases

Oracle, Obj

Chapter 7

Performance of 1998 Test Installation

In 1998, one arm of the Spectrometer was installed using preliminary designs for all components in order to test the feasibility an energy measurement using this approach. There were four primary goals for this installation:

- to measure the thermal and mechanical stability of the system,
- to measure the resolution of the BPMs,
- to commission the Data Acquisition and Storage software, and
- to find as many surprises as possible in the behaviour of the components in order to have a mature design ready for 1999.

After much effort, all the goals were met, although the number of surprises was a bit larger than we had hoped! This chapter presents a summary of the results obtained after an analysis of the 1998 data. As will be seen, all systems achieved their design resolutions in one way or another. The crucial test of stability between different beam energies was not performed, however, and will have to wait for the improvements designed into the 1999 installation.

7.1 Mechanical Stability

Tests of the mechanical stability of the components could only be carried out once the stability and resolution of the stretched-wire system could be measured, since this system provides the reference against which all other motions are measured.

7.1.1 Wire System Resolution

The intrinsic resolution of the sensor heads was tested shortly after installation in LEP. Figures 7.1 and 7.2 show data for each sensor taken with no beam in LEP and at a

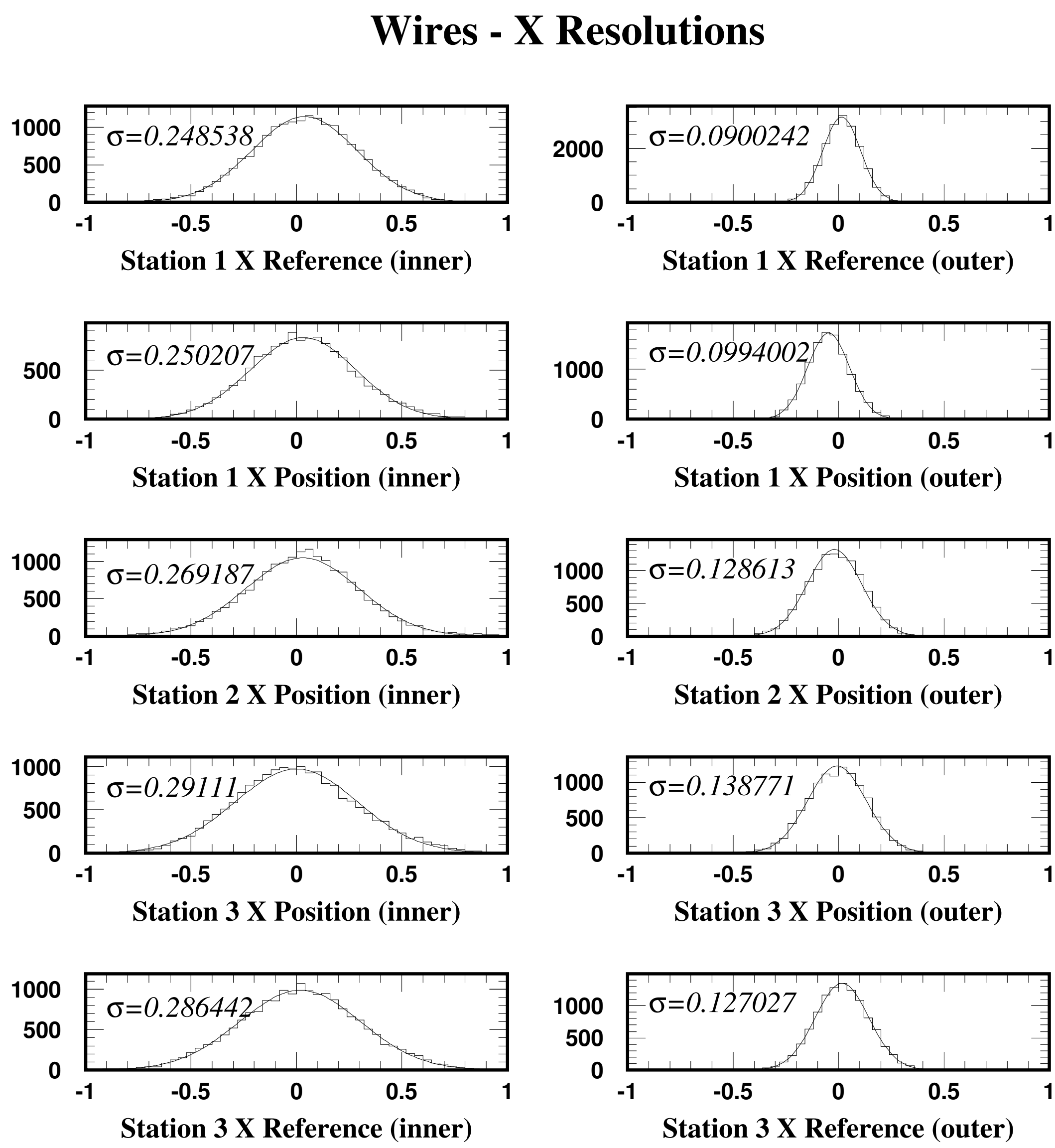

Figure 7.1: The resolution of the wire sensors in the horizontal plane as measured during running at 45 GeV in 1998. The left column of plots corresponds to the 5 sensors on the inside of the LEP ring, which observe the 30 meter long wire. The right column of plots represents those sensors on the outside of the LEP ring, on the shorter wire. The horizontal scale and the resolution derived from a gaussian fit to each plot is in microns.

constant temperature for the horizontal and vertical planes, respectively. The intrinsic resolution of the best sensors approaches 150 nm, whereas the largest resolution is around 400 nm. This is certainly sufficient for our purposes, if it can be maintained during LEP running conditions.

Some interesting features were discovered at very small levels; for example, a very slow oscillation of the multiple-kilogram counterweights could be seen in the wire positions. In

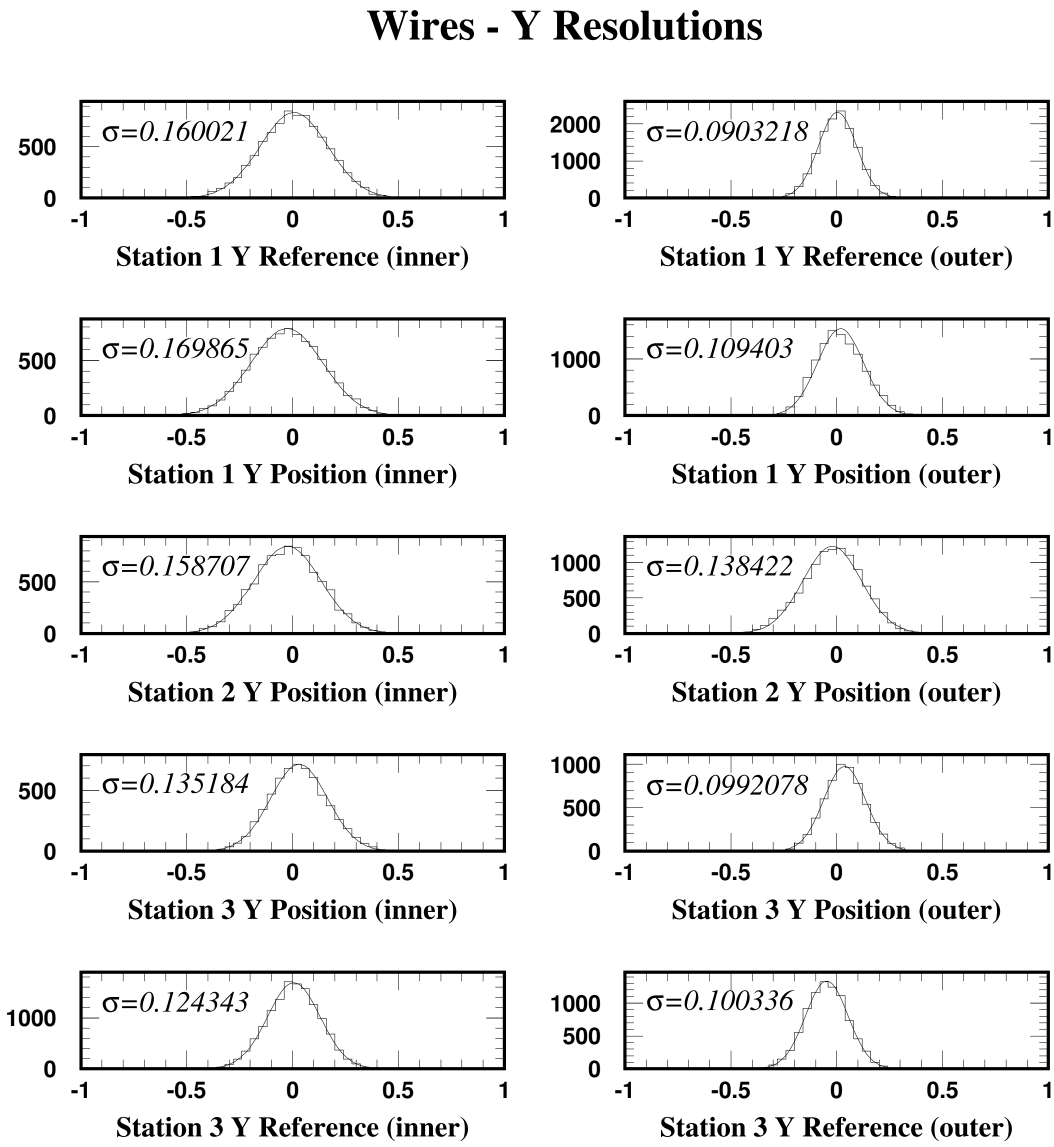

Figure 7.2: The resolution of the wire sensors in the vertical plane as measured during running at 45 GeV in 1998. The left column of plots corresponds to the 5 sensors on the inside of the LEP ring, which observe the 30 meter long wire. The right column of plots represents those sensors on the outside of the LEP ring, on the shorter wire. The horizontal scale and the resolution derived from a gaussian fit to each plot is in microns.

principle, some of these effects can be removed from the system. Since their amplitudes tend to be less than 100 nm, however, the overall effect is small.

7.2 BPM Resolution

Chapter 8

The MBI Field Map

8.1 The Mapping Bench and Arm

8.2 The Field Map

8.3 Systematic Errors of the Field Map

Chapter 9

Measurement Strategy and Prospects

Chapter 10

Schedule and Budget

Bibliography

[1] S. Eidelmann and F. Jegerlehner, Z. Phys. **C67** (1995) 585.

[2] R. M. Barnett *et al.*, Phys. Rev. **D54** (1996) 1.

[3] "A Combination of Preliminary Electroweak Measurements and Constraints on the Standard Model", LEP Electroweak Working Group, CERN/EP/99-XX.

[4] OPAL Collaboration, K. Ackerstaff *et al.*, Phys. Lett. B. **389** (1996) 416;
DELPHI Collaboration, P. Abreu *et al.*, Phys. Lett. B. **397** (1997) 158;
L3 Collaboration, M. Acciarri *et al.*, Phys. Lett. B. **398** (1997) 223;
ALEPH Collaboration, R. Barate *et al.*, Phys. Lett. B. **401** (1997) 347.

[5] L3 Collaboration, M. Acciarri *et al.*, Phys. Lett. B. **413** (1997) 176;
OPAL Collaboration, K. Ackerstaff *et al.*, Eur. Phys. J. C **1** (1998) 395;
DELPHI Collaboration, P. Abreu *et al.*, Eur. Phys. J. C **2** (1998) 581;
ALEPH Collaboration, R. Barate *et al.*, Phys. Lett. B. **422** (1998) 384.

[6] OPAL Collaboration, G. Abbiendi *et al.*, CERN-EP/98-197, Submitted to Phys. Lett. B

[7] "Evaluation of the LEP centre-of-mass energy above the W-pair production threshold", LEP Energy Working Group, CERN-EP/98-191, CERN-SL/98-073, Submitted to Eur. Phys. J. C.

[8] "Calibration of centre-of-mass energies at LEP1 for precise measurements of Z properties", LEP Energy Working Group, Eur. Phys. J. C 6 (1999) 2, 187-223.

[9] L. Arnaudon *et al.*, "Accurate determination of the LEP beam-energy by resonant depolarization", Z. Phys. C66 (1995) 45

[10] P.S. Wells, for The LEP Energy Working Group, private communication in preparation.

[11] Some EPAC reference on BPM electronics